A focal mechanism catalogue of earthquakes that occurred in the southeastern Alps and surrounding areas from 1928 – 2019

Angela Saraò, Monica Sugan, Gianni Bressan, Gianfranco Renner, Andrea Restivo[1*]

[1]National Institute of Oceanography and Applied Geophysics – OGS, Italy

Correspondence to: Angela Saraò (asarao@inogs.it)

Abstract. We present a focal mechanism catalogue of earthquakes that occurred in the southeastern Alps and surrounding areas from 1928 to 2019. The area involved in the process of convergence between the Adria microplate and Eurasia is one of the most seismically active regions in the Alpine Belt. The seismicity is minor, with the Ms=6.5 Friuli earthquake being the strongest event recorded in the area, but the seismic hazard is relevant because it is a highly populated region. For this reason, numerous studies have been carried out over time to investigate the stress field and the geodynamic characteristics of the region using focal mechanisms. To provide a comprehensive set of revised information, which is challenging to build quickly because the data is dispersed over many papers, we collected and revised the focal mechanisms that were previously published in the literature. Additionally, depending on the data quality and availability, we computed new focal mechanisms by first arrival polarity inversion or seismic moment tensor. Finally, we merged all the fault plane solutions to obtain a catalogue for a selection of 772 earthquakes with $1.8 \leq M \leq 6.5$. For each earthquake, we reported all the available focal mechanisms obtained by different authors. We also suggested a preferred solution for users who need expeditious information.

The catalogue described in this paper is available at http://doi.org/10.5281/zenodo.4660412 (Saraò et al., 2021) and will be updated periodically (https://doi.org/10.5281/zenodo.4284970).

1 Introduction

The focal mechanisms, or fault plane solutions (FPS), describe the orientation of the fault on which an earthquake occurs and the direction of the slip. FPS allow to understand seismotectonic processes through the study of the stress field of a region, and are essential for seismic hazard assessment.

[1*] Andrea Restivo passed away on 24 August 2020

25 The first methods to determine the FPS (Knopoff and Gilbert, 1960) were based on observations of the polarity of the first P wave motion at stations placed at known distances and azimuths from the source.

After the 1980s, with the development of digital broadband instruments, FPS computed by the seismic moment tensors became very popular (e.g., Gilbert, 1970; Dziewonski et al., 1981). The point source is located at the hypocentre, except for models that make use of the source centroid. The difference between the location of the initiation of rupture and the centroid can be

30 significant, except for that of small earthquakes (Dziewonski and Woodhouse, 1983). For this reason, FPS computed by polarities or by moment tensors might produce different results, not only due to systematic errors or inadequacies in the velocity models. The use of mechanisms by polarities represent the geometry of the fault at the initial breaking of the rupture, while the moment tensor provides the source mechanism of the dominant component of the rupture geometry. Additionally, the differences between the two methods become relevant when the source deviates by the approximation of a pure double couple,

35 for instance, when fluids play an essential role in earthquake generation. However, despite their limits - such as inadequacies in the P- and S-wave velocity models and poor station coverage, together with erroneous polarity readings that may result in large deviations between the model solution and the actual fault planes - the focal mechanisms using first motion polarities are still computed and used. For small to moderate earthquakes (i.e. aftershock sequences), often they are the only source information available obtained using local network data (Shearer, 1998, Lentas et al., 2019).

40

At present, almost all seismological observatories compute quick moment tensors for earthquakes above a certain threshold of magnitude and publish solutions on dedicated online platforms. The Global Centroid-Moment-Tensor (CMT) Project (Dziewonski et al., 1981; Ekström et al., 2012), the National Earthquake Information Center (NEIC) of the USGS (Benz, 2017) and the GEOFON data centre (2020) report moment tensor solutions for world seismicity and thresholds of magnitudes of

45 about Mw 5.0, Mw 5.5 and Mw 4.5 respectively. In addition to these, there are also many regional or local moment tensor catalogues with magnitude thresholds of about Mw 3.6 (e.g Scognamiglio et al., 2006 [Time Domain Moment Tensor catalogue – TDMT]; Kubo et al., 2002 [NIED seismic moment tensor catalogue) and Mw 4.5 (e.g. Pondrelli and Salimbeni 2015 [Regional Centroid Moment Tensor Catalog – RCMT]. Furthermore, some online databases, such as the bulletin of the International Seismological Centre (Lentas et al., 2019) or the database of the Stress World Map project (Zoback, 1992;

50 Heidbach et al., 2018), contain both polarities and moment tensor FPS of global seismicity.

In the past, the FPS were computed and published in specific studies investigating the geodynamics of specific regions. These studies are still being performed today to revise the preliminary FPS or calculate the FPS of events of M < 4.0. Several authors have put considerable effort into researching FPS reported in many papers and collecting them in catalogues for specific areas to provide a set of revised information, which is often challenging to build quickly. Valuable to stress that collecting data, very

55 often spread in different documents and locations, checking and selecting parameters, standardize the information is a long and painstaking job, sometimes not fully known.

For European areas, in addition to the first compilations of Constantinescu et al. (1966), McKenzie (1972) and Udías et al. (1989), more recent catalogues include the EMMA database (Vannucci and Gasperini, 2004), which collects the focal

mechanisms of earthquakes that occurred in the Mediterranean area from 1905 to 2006 in the range $4 \leq Mw \leq 8.7$. In several cases, after merging the available FPS for an earthquake, the authors assess and suggest a preferred solution based on different priorities or strategy (e.g. Gerner, 1995; Radulian et al., 2002; Custódio et al., 2016; Kapetanidis and Kassaras, 2019).

In this study, we present a new catalogue of FPS of earthquakes that occurred in the southeastern Alps and surrounding areas from 1928 to 2019 (Saraò et al., 2020). Because of the relevant seismic hazards (e.g., Slejko et al., 1998; Meletti et al., 2021) and its importance from a geodynamical point of view, many authors have computed the FPS of earthquakes that occurred in this area using different data and different techniques (e.g., Anderson and Jackson, 1987; Slejko et al., 1989; Del Ben et al., 1991; Herak et al., 1995; Bernardis et al., 1997; Slejko et al., 1999; Aoudia et al., 2000; Pondrelli et al., 2001; Poli and Renner 2004; Danesi et al., 2015; Viganò et al., 2008; Bressan et al., 2007; 2009; 2018; Pondrelli and Salimbeni 2015; Restivo et al., 2016; Romano et al., 2019). A significant boost in seismological studies of the area occurred after the devastating 1976 Friuli earthquake (Ms=6.5), the strongest earthquake recorded in instrumental times in northeastern Italy (Slejko et al., 2018 and reference therein). In addition to the mainshocks, the most energetic aftershocks (e.g., Slejko et al., 1989; Slejko et al., 1999; Poli et al., 2002) were analysed to understand the geodynamic process occurring in the area; most of the FPS of the Friuli sequence were calculated manually using a graphical method. Subsequently, with the use of computer techniques (Whitcomb 1973; Reasenberger and Oppenheimer, 1985), many other small earthquakes belonging to the seismic sequences occurring in the area (e.g., Bernardis et al., 1997; Bressan et al., 2009; 2018) were carefully investigated to understand the stress regime of the area (e.g., Bressan et al., 2003; 2007; 2009; 2018). In recent times, Aoudia et al. (2000) and Pondrelli et al. (2001) reviewed the mechanisms of 1976 mainshocks in terms of the moment tensor, and since 2006, the moment tensor has been routinely computed for earthquakes M≥3.6 in the region (e.g., Scognamiglio et al., 2009; Saraò, 2016).

The aim of our study is to collect and revise all the FPS published for the area over time in a comprehensive catalogue. Additionally, we employ a set of first polarity data collected by an author before data exchange via the Internet and visit select observatories to analyse the seismograms. These data were used to compute the FPS manually in previous studies, but only portions of them were published. We use the datasets to recalculate the FPS based on current knowledge (Sugan et al., 2020). The new solutions are then merged with the FPS found in the literature. Depending on the data availability and quality, we compiled a dataset with the FPS computed for 772 selected earthquakes (Saraò et al., 2020). In the following section, we describe the study area, the methodologies and data used to build our catalogue and outline its main characteristics.

2 The study area

The region that we considered in this study (Fig. 1) is bounded by Garda Lake to the west, Western Slovenia to the east, the Venetian Po Plain to the south and Austria to the north (latitude 45°N-47.5°N and longitude 10°E-15°E). The area is one of the most seismically active regions of the Alpine Belt and is involved in the convergence between the Adria microplate and Eurasia (e.g., Battaglia et al., 2004; D'Agostino et al., 2005, 2008; Serpelloni et al., 2005). The rates of convergence increase from west to the east by up to 1.5 mm/yr. to 2.0 mm/yr. (D'Agostino et al., 2005). The structural setting is a complex system

resulting from the superposition of several tectonic phases that have generated a NW-SE-trending Dinaric chain (to the east) and E-W-trending Alpine faults (southeastern Alps). On the west, the Giudicarie-Lessini region is a crucial zone for geodynamics, and it represents a tectonic boundary between the central-western and eastern Southern Alps with an orientation transverse to the strike of the Alpine chain (Viganò et al., 2015).

95   The National Institute of Oceanography and Applied Geophysics (OGS) northeastern Italy seismic and deformation network (Priolo et al., 2005; Bragato et al., 2011, Bragato et al., 2021) has monitored the study region since 1977, complemented since 2002 by a GNSS network (Zuliani et al., 2018). Several studies (e.g., Gentili et al., 2011; Peruzza et al., 2015 and Sandron et al., 2018) provide a general description of the data recorded, including the main variations of the OGS North-Eastern Italy (OX) network geometry over time, the acquisition mode and the type of seismographs.

100   The seismicity, mainly located in the upper crust (Bressan et al., 2018, 2019; Viganò et al., 2015), is minor and directly related to the deformation along the western margin of the Adriatic indentation (Gentili et al., 2011; Romano et al., 2019). Rovida et al. (2020) reported that approximately thirty earthquakes of $5.5 \leq M \leq 6.5$ occurred in historical time, and the largest mainshocks (M>5.0) instrumentally recorded after the 1976 Ms=6.5 Friuli earthquakes (e.g., Aoudia et al., 2000) occurred in the 1998 Ms=5.7 and 2004 M_w=5.1 in the Bovec area (e.g., Bajc et al., 2001; Kastelic et al., 2008; Bressan et al., 2009) (Fig.

105   1).

3 Methodology

3.1 FPS from the literature

The FPS from the literature were obtained after careful research; the found FPS were thoroughly checked for typos and orthogonality of the nodal planes as well as for the compatibility of pressure and tension axes with the nodal planes according

110   to the Aki and Richards (1980) convention. The Aki and Richards (1980) convention defines the two planes by the strike, measured clockwise from the north, with the fault dipping down to the right of the strike direction, and the dip, measured down from the horizontal. The rake is the angle between the strike direction and slip, where slip is taken as the direction of the hanging wall relative to the footwall. Because the two planes are orthogonal, the three angles defining one plane also define the orientation of the second plane. The orientations of the pressure (P) and tension (T) axes, located in the centre of the

115   dilatational and compressional quadrants, respectively, are given by the azimuth (0-360°, North =0°, East=90°) and the plunge (0-90°, down from the horizontal).

Starting with the published nodal planes, we recomputed the solutions to check their consistency and to add, when missing, a uniform dataset of parameters for each event. Whenever possible, we cross-checked the corrected solutions with the author or the beach ball shown in the original publication. We did not include the solutions for which it was impossible to recover

120   consistent planes starting from the available information in the catalogue. In the case of multiple FPS for the same earthquake, we considered all of them. However, when the FPS were copied from one paper to another by different authors, we reported

the FPS referred to in the first article they appeared. If the same authors published slightly different FPS for the same earthquake, we considered only the FPS of the most recent publication.

3.2 The new computed FPS

125 Before computing the FPS, we relocated the earthquakes using Hypo71 (Lee and Lahr, 1975), a standard location procedure, and the 1D layered velocity model (Riggio and Russi, 1984; Bressan et al., 2003) used for the analysis of the earthquake reported in the Friuli-Venezia Giulia Seismometric Network Bulletin (2020). The model had a P-wave velocity (Vp) = 5.85 km/s from the surface down to a depth of 22 km, a Vp = 6.8 km/s from 22 to 39.5 km depth and a Vp=8 km/s for the half-space. The P to S-wave velocity ratio is 1.78.

130 To estimate the FPS by polarities, we used the FPFIT algorithm (Reasenberger and Oppenheimer, 1985), which is based on a grid-search procedure that finds the strike, dip and rake of the two planes by minimizing a normalized weighted sum of the first-motion polarity discrepancies. The misfit function (zero perfect fit, one complete misfit) is computed from the number of inconsistent polarities and weighted by the quality of the observation and the distance from the nodal planes. For some events, the inversion program provided multiple solutions as a result of an insufficient number of polarity readings, the presence of

135 polarity misreading, the inclusion of localization errors or the use of an inadequate velocity model. In such cases, we selected the preferred solution based on a) the data distribution on the focal sphere relative to the radiation pattern (i.e., number of first motion polarities - FM $\geq$ 10; station distribution ratio - STDR $\geq$ 0.4; Misfit $\leq$ 0.3) and b) agreement with the tectonic lineaments and style of the epicentral area.

The first polarities used to compute the FPS were manually picked from seismograms or extracted from the *Bulletin of the*

140 *International Seismological Centre* and the *Seismological Bulletin of Slovenia*. The polarities were also read from the seismograms archived in various Italian and European seismological observatories, many of which are no longer operating (*Osservatorio meteorico-sismico nel Seminario - Chiavari; ENEL, Osservatorio Ximeniano - Florence, Osservatorio Astronomico "Brera" - Milan, Dipartimento di Fisica dell'Università di Padova - Padua, Osservatorio S. Domenico – Prato, Osservatorio meteoro-sismico nel Santuario di N.S. - Oropa, Osservatorio Bina - Perugia, Osservatorio "Valerio"- Pesaro,*

145 *Osservatorio meteorico-sismico nel Collegio Alberoni - Piacenza, Osservatorio Meteorico Istituto Fisica - University of Siena, Sismografi Lungo Periodo di Mantovani (Bologna, Bolzano, Grosseto, Naples, Olbia, Palermo, Turin), Osservatorio meteorico-sismico nel Seminario Maggiore - Treviso, Osservatorio meteorico-sismico nel Seminario Patriarcale – Venice, Ljubljana, Munich, Stuttgart, Vienna).*

After 1977, the first motion polarities were also picked from the seismograms recorded by the network managed by OGS and

150 integrated with the data recorded by the surrounding seismic networks. Since 2006, we used the digital seismograms acquired by the OX network to compute the seismic moment tensor for earthquakes $M_L \geq 3.6$ that occurred in NE Italy and the strict surroundings (Bragato et al., 2011; Saraò et al., 2016, Saraò, 2020). Using the TDMT code by Dreger (2003), an algorithm widely employed in several observatories worldwide (e.g., Kubo et al., 2002; Clinton et al., 2006; Scognamiglio et al., 2009), we inverted the seismic waveforms in the frequency range of 0.02 - 0.05 Hz. A cross-correlation function was used to align

155 data with Green's functions computed by the algorithm of Saikia (1984). This level of approximation afforded a great level of flexibility in rapid source parameter determinations when the event locations and the origin time are preliminary (Dreger and Helmberger, 1993; Dreger et al., 1998). The source depth is estimated iteratively by finding the solution that yields the highest variance reduction (VR). VR is an index of the waveform fit between observed and synthetic seismograms and is given by the sum of squares of the difference in amplitude normalized by the observed waveforms (where 100% is best). Kubo et al. (2002)

160 showed that stable and reliable solutions are obtained for VR greater than 50%.

Noisy or nodal stations and inadequate structural models can result in inaccurate moment tensor estimates. For this reason, Saraò (2007) performed a feasibility study to calibrate and tune the algorithm for the investigated area in relation to the station geometry and to the local velocity model employed (Bressan, 2005), finding the best parameter configuration that allows robust estimates of the best double couple orientation and of the M_w value.

165 **3.3 Merging the new FPS with the published ones**

Although we reported all the available FPS for an earthquake in the catalogue, both retrieved from the literature or newly computed, we indicated a preferred one based on the following priority criteria: 1) the solution was computed within this study; 2) the fault plane solution was determined by moment tensor; 3) the solution was computed in the framework of a detailed study of the area and possibly after accurate relocation of the hypocentre. In both these cases, each fault plane solution was

170 validated for data quality and distribution; 4) the solution is the latest computation; 5) the solution is compatible with our knowledge of the main tectonic features of the area: 6) the solution is part of a regional catalogue; 7) the solution is compatible with most of the solutions proposed by independent studies It was impossible to select the best solution based on the quality parameters of the FPS computation because such parameters were computed in a heterogeneous way and are provided sporadically.

175 To account for the variability of the preferred solution and the alternative ones (i.e. solutions of other authors) for the same event, we computed the 3D rotation angle by which one double couple was rotated into another arbitrary couple (Kagan, 1991). The Kagan angle varies between 0° for identical solutions and 120° for the absolute mismatches. Pairs of solutions with an angle below 20°-30° were considered very similar (Nakamura et al., 2016; Lentas et al., 2019).

We used the software FMC (Álvarez-Gómez, 2019), which includes subroutines from Gasperini and Vannucci (2003), to

180 verify and classify all the focal mechanisms in our catalogue. The fault type was classified by seven types of double couple classification (N: Normal; N-SS: Normal - Strike-slip; SS-N: Strike-slip - Normal; SS: Strike-slip; SS-R: Strike-slip - Reverse; R-SS: Reverse - Strike-slip; R: Reverse) similar to the conceptual geological classification of faults (Álvarez-Gómez , 2019). To provide thorough information and facilitate easy inclusion in other databases, we also reported the classification adopted by the World Stress Map Project (Zoback 1992). This classified the events into five types (N, N-SS, SS, R-SS, R), and those

185 not fitting in any of the five types were placed in the unknown category.

4 Analysis of the catalogue and discussion

We report in our catalogue 987 fault plane solutions for 772 earthquakes (Fig. 2) with a magnitude range of $1.8 \leq M \leq 6.5$ (Saraò et al., 2020). For each earthquake, we report the latitude and longitude of the epicentre, origin time, focal depth, magnitude, the strike, dip, rake of the two nodal planes, azimuth and plunge of the P, T, and B axes, fault type (using both Alvarez-Gomez, 2019 and Zoback 1992 classifications), Kagan angle and associated references. In the case of multiple solutions, we indicate the preferred one, and the classification according the priority code described in the previous section.

We collected and revised from the literature 836 FPS (85% of the whole catalogue), 68 of which have been corrected with respect to the original information, while for 428 we added the values missing to obtain a uniform dataset of information. For each solution, the changes reported are commented in the database. Of the 151 newly computed focal mechanisms reported in the catalogue, 108 earthquakes with $1.8 \leq M \leq 4.8$ occurring between 1928 and 2019 are computed by first motion polarities (Table 1, Sugan et al. 2020 for details of the input data and inversion results), and 43 earthquakes with $3.4 \leq M_w \leq 5.1$ occurring from 2002 to 2018 are computed by moment tensor (Table 2, Saraò 2020, for details of the solutions).

The focal mechanisms are provided for selected earthquakes that occurred in the area based on data availability and quality, although since 1976, the MT is available by international agencies (e.g., CMT and RCMT) for all earthquakes $M \geq 4.5$, and since 2006, we compute the MT for all earthquakes of $M \geq 3.6$ and we publish the results online (RTS, 2020). For such reasons, the distribution in time and magnitude of the mechanisms of our catalogue may be uneven and linked to the study case of specific earthquakes and particular seismic sequences. Looking at the temporal distribution of the FPS of our catalogue (Fig. 3), we observe peaks in seismicity following the 1976 Ms=6.5 Friuli earthquake, 1998 M_S=5.7 earthquake (Bajc et al., 2001) and 2004 M_w=5.1 2004 Bovec earthquakes (e.g., Bressan et al., 2007; 2009). The increasing number of focal mechanisms soon after the 1976 Friuli earthquake was boosted both by data coming from temporary stations (Slejko et al., 1999) and by the development of the OGS networks that has since then made it possible to investigate small energy earthquakes (M< 3.5). The magnitude of the computed FPS ranges from 1.8 to 6.5, but most of the fault plane solutions have been computed in the magnitude range of 2.8 to 3.5 (Fig. 4).

The ternary diagram of Fig. 5 shows the fault type distribution of the 772 preferred FPS contained in our catalogue, while the pie plots (Fig. 6a, 6b) show the percentage of fault type mechanisms obtained by the two approaches to classify the mechanisms. The classification by Álvarez-Gómez (Fig. 6a) accurately characterize seismic earthquakes with different strike-slip components. Reverse mechanisms feature the area under investigation, but the presence of strike-slip solutions is also relevant and in agreement with the different kinematic regimes that characterize the region from east to west. Previous studies (e.g., Slejko et al., 1999; Poli et al., 2002; Bressan et al., 2018) have shown that thrust faulting is the dominant mechanism on the southeastern Alps showing a significant presence of strike-slip events, while strike-slip faulting prevails in the Dinaric domain. Viganò et al. (2015) found that thrust faults with a strike-slip component and strike-slip faults prevail in the western sector, confirming that the seismotectonic zones Giudicarie and Lessini are undergoing different kinematic regimes.

7

In Fig. 7, we plot the Kagan angle to show the difference between our preferred solutions and the other FPS available for the same earthquake. Although many pairs of focal mechanisms are below 20°-30°, there are discrepancies above 30°. The observed trend is not surprising and has been found for other datasets with multiple earthquake source solutions (e.g., Ishibe et al., 2014; Nakamura et al., 2016; Lentas et al., 2019) due to the differences in data and methods used to compute the solution for the same earthquake over time.

From the comparison of the solutions computed in this study with solutions already published, we observe some agreement but also some discrepancies that are likely due to the different configuration parameters used to locate the events, the different datasets used as input and the diverse techniques employed.

For instance, the location of the 1928 Ms=5.8 Tolmezzo earthquake, the oldest event in our dataset (Table 1), is different from that of previous studies (e.g., Slejko et al., 1989; Sandron et al., 2018), and it is more compatible both with the location reported in the macroseismic Italian database and associated catalogue (Locati et al., 2016, Rovida et al., 2020; 2021) and with the seismogenic features of the area than before (Bressan et al., 2018). Recently Rovida et al. (2021) has revised the magnitude for this event to be equal to 6.08. The retrieved focal mechanism is a strike-slip type confirming the solutions previously found by other authors (e.g., Slejko et al., 1989; Cagnetti et al., 1976), probably because of the low impact of the hypocentral location when using data from very far-field stations, as was used in this case.

It is worth mentioning the results of the 1936 Ms=5.6 Alpago Cansiglio earthquake (Table 2), whose causative fault is still controversial (Galadini et al., 2005; Sugan and Peruzza 2011). We obtained two possible FPS (Sugan et al., 2020): one with a strike-slip component, as previously found by others (e.g., Peruzza et al., 1989), and one with a compressive solution compatible within the uncertainties with the mechanism obtained by Sirovich and Pettenati (2004) using the regional macroseismic intensity pattern. We suggest the compressive solution as the preferred one and hypothesize that the new solution can shed new light on the study of this earthquake being compatible with a known fault segment (Aviano Thrust outcropping) along the Cansiglio mountain front (Galadini et al., 2005).

5 Concluding remarks

We compiled a comprehensive catalogue of 987 focal mechanisms for 772 selected earthquakes of $1.8 \leq M \leq 6.5$ that occurred in the southeastern Alps and surrounding areas from 1928 to 2019 (Saraò et al., 2020). The study region represents a key area from a geodynamic point of view and is characterized by significant seismic risk, as reported in Italian seismic hazard maps. For such reasons, many authors have investigated the seismicity of this region, computing many focal mechanisms. In the catalogue, we have collected and revised 836 published solutions to provide a homogeneous and high quality dataset of focal mechanisms; 68 have been corrected for typos or inconsistencies, and, whenever possible, the corrected solutions have been discussed with the original author or checked against the available details in the paper. Additionally, we have enhanced and made available the set of polarities readings of past earthquakes that would otherwise be lost; thus, we computed 108 new FPS of earthquakes that occurred between 1928 and 2019 using a set of peak polarities readings that were not used or published

250   before for certain reasons (Sugan et al., 2020) and 43 earthquakes with $3.4 \leq Mw \leq 5.1$ that occurred from 2002 to 2018 by moment tensor (Saraò, 2020).

The distribution in time and magnitude of the FPS are correlated to the study cases of specific earthquakes (e.g., 1976 Ms=6.5 Friuli earthquake, 1998 Ms=5.7 and 2004 Mw=5.1 Bovec earthquakes) and relevant seismic sequences occurred in the area. Thrust faulting is the dominant mechanism of our catalogue, with a significant presence of strike-slip events and a minor

255   presence of normal faults. In the catalogue, we report all the FPS available for each earthquake, and we suggest a preferred FPS for users who need to quickly have information to roughly represent the area at the current state of knowledge. By the Kagan angle, we quantify the difference among the preferred solutions and other solutions to provide additional insights to the final user. If the differences are well within the uncertainties for the majority of focal mechanism pairs, the discrepancy might be relevant for some other cases.

260   Our catalogue, available at https://doi.org/10.5281/zenodo.4284970, will be upgraded yearly with the FPS of the most recent earthquakes occurring in the area to maintain the published dataset as up to date and complete as possible.

Data

The catalogue of focal mechanisms described in this paper is available at Zenodo (https://doi.org/10.5281/zenodo.4660412 , Saraò et al., 2021).

265   The first motion dataset used to compute the focal mechanisms is available at Zenodo (https://doi.org/10.5281/zenodo.4284929, Sugan et al., 2020).

The seismic data used to compute the seismic moment tensor are provided by the OGS North-East Italy Seismic Network (OX) https://doi:10.7914/SN/OX. The waveforms can be downloaded from the European Integrated Data Archive EIDA (http://www.orfeus-eu.org/data/eida/).

270

Author contributions

AS designed the experiment. AS and MS wrote the manuscript, prepared the figures and revised the FPS collected from the literature. MS, GB, GF, AR read the first arrival peaks and computed the new FPS by polarities. AS computed the FPS by moment tensor. GB provided comments on the paper.

275 **Competing interests**

The authors declare that they have no conflict of interest.

9

References

Álvarez-Gómez, J.A.: FMC - Earthquake focal mechanisms data management, cluster and Classification, SoftwareX, 9, 299–307, https://doi.org/10.1016/j.softx.2019.03.008, 2019.

290 Aki, K., Richards, P.G.: Quantitative seismology, Freeman, San Francisco, Vol. I and II, 932 pp., 1980.

Anderson, H., Jackson, J.: Active tectonics of the Adriatic Region, Geophys. J. R. Astron. Soc., 91, 937-983, https://doi.org/10.1111/j.1365-246X.1987.tb01675.x, 1987.

Aoudia, A., Saraò, A., Bukchin, B., Suhadolc, P.: The 1976 Friuli NE Italy thrust faulting earthquake: a reappraisal 23 years later, Geophys. Res. Lett., 27, 573-576, https://doi.org/10.1029/1999GL011071, 2000.

295 Bajc, J., Aoudia, A., Saraò, A., Suhadolc, P.: The 1998 Bovec-Krn (Slovenia) earthquake sequence, Geophys. Res. Lett., 28, 1839-1842, https://doi.org/10.1029/2000GL011973, 2001.

Battaglia, M., Murray, M.H., Serpelloni, E., Bürgmann, R.: The Adriatic region: an independent microplate within the Africa–Eurasia collision zone, Geophys. Res. Lett. 31, http://dx.doi.org/10.1029/2004GL019723, 2004.

Benz, H.: Building a National Seismic Monitoring Center: NEIC from 2000 to the Present, Seism. Res. Lett., 88, 457-461,
300 https://doi.org/10.1785/0220170034, 2017.

Bernardis, G., Poli, M.E., Renner, G., Snidarcig, A., Zanferrari, A.: Le tre sequenze sismiche del 1996 a Claut (Prealpi Carniche), in: Atti GNGTS, 15 Convegno, Roma, 343-348, 1997.

Bragato, P.L., Di Bartolomeo, P., Pesaresi, D., Plasencia Linares, M., Saraò A.: Acquiring, archiving, analyzing and exchanging seismic data in real time at the Seismological Research Center of the OGS in Italy, Ann. Geophys. 54, 67–75,
305 https://doi.org/10.4401/ag-4958, 2011.

Bragato P.L., Comelli, P., Saraò, A., Zuliani, D., Moratto, L., Poggi, V., Rossi, G., Scaini, C., Sugan, M., Barnaba, C., Bernardi, P., Bertoni, M., Bressan, G., Compagno, A., Del Negro, E., Di Bartolomeo, P., Fabris, P., Garbin, M., Grossi, M., Magrin, A., Magrin, E., Pesaresi, D., Petrovic, B., Plasencia Linares, M.P., Romanelli, M., Snidarcig, A., Tunini, L., Urban, S., Venturini, E., Parolai, S.: The OGS- North-Eastern Italy Seismic and Deformation Network: current status and outlook. Seism. Res. Lett., https://doi.org/10.1785/0220200372, 2021.

Bressan, G.: Modelli di velocità 1D dell'Italia Nord Orientale, Internal report OGS (in Italian) CRS/5/20/2005, Udine, 18 pp., 2005.

Bressan, G., Bragato, P.L., Venturini, C.: Stress and strain tensors based on focal mechanisms in the seismotectonic framework of the Friuli–Venezia Giulia region (north-eastern Italy), Bull. Seism. Soc. Am., 93, 1280-1297, https://doi.org/10.1785/0120020058, 2003.

Bressan, G., Kravanja, S., Franceschina, G.: Source parameters and stress release of seismic sequences occurred in the Friuli-Venezia Giulia region (Northeastern Italy) and in Western Slovenia, Phys. Earth Planet. Int., 160, 192-214, https://doi.org/10.1016/j.pepi.2006.10.005, 2007.

Bressan, G., Gentile, G.F., Perniola, B. Urban, S.: The 1998 and 2004 Bovec-Krn (Slovenia) seismic sequences: aftershock pattern, focal mechanisms and static stress changes, Geophys. J. Int., 179, 231–253, https://doi.org/10.1111/j.1365-246X.2009.04247.x, 2009.

Bressan, G., Barnaba, C., Bragato, P., Ponton, M.,Restivo, A.: Revised seismotectonic model of NE Italy and W Slovenia based on focal mechanism inversion, J. Seismol., 22, 1563-1578, https://doi:10.1007/s10950-018-9785-2, 2018.

Bressan, G., Barnaba, C., Bragato, P.L., Peresan, A., Rossi, G., Urban, S.: Distretti sismici del Friuli Venezia Giulia, Boll. Geof. Teor. Appl., 60, suppl.3, pp. s1-s74, DOI 10.4430/bgta0300, 2019.

Cagnetti, V., Pasquale, V., Polinari, S.: Focal mechanisms of earthquakes in Italy and adjacent regions, CNEN Rt/Amb 76, 4, Roma, 41 pp, 1976.

Clinton, J. F., Hauksson E., Solanki, K.: An Evaluation of the SCSN Moment Tensor Solutions: Robustness of the Mw Magnitude Scale, Style of Faulting, and Automation of the Method, Bull. Seism. Soc. Am., 96, 1689-1705, http://doi.org/10.1785/0120050241, 2006.

Constantinescu, L., Ruprechtová, L., Enescu, D.: Mediterranean-Alpine Earthquake Mechanisms and their Seismotectonic Implications, Geophys. J. Int., 10, 347–368, https://doi.org/10.1111/j.1365-246X.1966.tb03063.x, 1966.

Custódio, S., Lima, V., Vales, D., Cesca, S., Carrilho, F.: Imaging active faulting in a region of distributed deformation from the joint clustering of focal mechanisms and hypocentres: application to the Azores–western Mediterranean region, Tectonophysics 676, 70–89, https://doi.org/10.1016/j.tecto.2016.03.013, 2016.

D'Agostino, N., Cheloni, D., Mantenuto, S., Selvaggi, G., Michelini, A., Zuliani, D.: Strain accumulation in the Southern Alps (NE Italy) and deformation at the northeastern boundary of Adria observed by CGPS measurements., Geophys. Res. Lett., 32, http://dx.doi.org/10.1029/2005GL024266, 2005.

D'Agostino, N., Avallone, A., Cheloni, D., D'Anastasio, E., Mantenuto, S., Selvaggi, G.: Active tectonics of the Adriatic region

340 from GPS and earthquake slip vectors, J. Geophys. Res., 113, https://doi.org/10.1029/2008JB005860, 2008.

Danesi, S., Pondrelli, S., Salimbeni, S., Cavaliere, A., Serpelloni, E., Danecek, P., Lovati, S., Massa, M.: Active deformation and seismicity in the Southern Alps (Italy): The Montello hill as a case study, Tectonophysics, 653, 95-108, https://doi:10.1016/j.tecto.2015.03.028, 2015.

Del Ben, A., Finetti, I., Rebez, A., Slejko, D.: Seismicity and seismotectonics at the Alps-Dinarides contact, Boll. Geof. Teor.

345 Appl., 33, 130-131, 155-175, 1991.

Dreger, D., Helmberger, D.V.: Determination of source parameters at regional distances with three component sparse network data, J. Geophys. Res., 98, 8107-8125, 1993.

Dreger, D., Uhrhammer, R., Pasyanos, M., Franck, J., Romanowicz, B.: Regional and Far-Regional Earthquake Locations and Source Parameters Using Sparse Broad Band Networks: A test on the Ridgecrest Sequence, Bull. Seism. Soc. Am., 88, 1353-

350 1362, 1998.

Dreger, D. S.: TDMT_INV: Time Domain Seismic Moment Tensor INVersion, International Handbook of Earthquake and Engineering Seismology, 81B, p 1627, 2003.

Dziewonski, A.M., Chou, T.A., Woodhouse, J.H.: Determination of earthquake source parameters from waveform data for studies of global and regional seismicity, J. Geophys. Res., 86, 2825-2852, https://doi.org/10.1029/JB086iB04p02825, 1981.

355 Dziewonski, A. M. and Woodhouse, J. H.: An experiment in systematic study of global seismicity: centroid-moment tensor solutions for 201 moderate and large earthquakes of 1981, J. Geophys. Res., 88, 3247–3271, 1983.

Ekström, G., Nettles, M., and Dziewonski, A.M.: The global CMT project 2004-2010: Centroid-moment tensors for 13,017 earthquakes, Phys. Earth Planet. Inter., 200-201, https://doi.org/10.1016/j.pepi.2012.04.002, 2012.

Friuli-Venezia Giulia Seismometric Network Bulletin: http://www.crs.inogs.it/bollettino/RSFVG/RSFVG.en.html, last

360 access: 22 September, 2020.

Galadini, F., Poli, M.E., Zanferrari, A.: Seismogenic sources potentially responsible for earthquakes with M ≥ 6 in the eastern Southern Alps (Thiene-Udine sector, NE Italy), Geophys. J. Int., 161, 739-762, https://doi.org/10.1111/j.1365-246X.2005.02571.x, 2005.

Gasperini, P, Vannucci, G.: FPSPACK: A package of FORTRAN subroutines to manage earthquake focal mechanism data.

365 Comput. Geosci., 29, 893–901. http://dx.doi.org/10.1016/S0098-3004(03)00096-7, 2003.

Gentili, S., Sugan, M., Peruzza, L., Schorlemmer, D.: Probabilistic completeness assessment of the past 30 years of seismic monitoring in northeastern Italy, Phys. Earth Planet. Inter., 186, 81-96, https://doi.org/10.1016/j.pepi.2011.03.005, 2011.

GEOFON, Data centre. GEOFON Moment Tensor Solutions: http://geofon.gfz-potsdam.de/eqinfo/list.php?mode=mt, last access: 03 November 2020.

370 Gerner, P.: Catalogue of Earthquake Focal Mechanism Solutions for the Pannonian Region, Geophysical Department, Eötvös University, Budapest, pp. 38, 1995.

Gilbert, F.: Excitation of the normal modes of the Earth by earthquakes sources., Geophys. J. Roy. Astr. Soc., 22, 223–226, https://doi.org/10.1111/j.1365-246X.1971.tb03593.x, 1970.

375 Heidbach, O., Rajabi, M., Cui, X., Fuchs, K., Müller, B., Reinecker, J., Reiter, K., Tingay, M., Wenzel, F., Xie, F., Ziegler, M.O., Zoback, M.L., Zoback, M.D.: The World Stress Map database release 2016: Crustal stress pattern across scales, Tectonophysics, 744, 484-498, https://doi.org/10.1016/j.tecto.2018.07.007, 2018.

Herak, M., Herak, D., Markusic, S.: Fault plane solution for earthquakes (1956–1995) in Croatia and neighbouring regions, Geofizika, 12, 43–56, 1995.

Ishibe, T., Tsuruoka, H., Satake, K., Nakatani, M.: A Focal Mechanism Solution Catalog of Earthquakes ($M{\geq}2.0$) in and around
380 the Japanese Islands for 1985–1998, Bull. Seism. Soc. Am., 104, 1031-1036, doi: 10.1785/0120130278, 2016.

International Seismological Centre, Seismological Dataset Repository: https://doi.org/10.31905/6TJZECEY, last access: 12 July 2020.

Kagan, Y. Y.: 3-D rotation of double-couple earthquake sources, Geophys. J. Int., 106, 709–716, https://doi.org/10.1111/j.1365- 246x.1991.tb06343.x, 1991.

385 Kapetanidis, V., Kassaras, I.: Contemporary crustal stress of the Greek region deduced from earthquake focal mechanisms, Journal of Geodynamics, 123, 55–82, 2019.

Kaverina, A.N., Lander, A.V., Prozorov, A.G.: Global creepex distribution and its relation to earthquake-source geometry and tectonic origin, Geophys. J. Int., 125, 249–265, https://doi.org/10.1111/j.1365-246X.1996.tb06549.x, 1996.

Knopoff, L., Gilbert, F.: First motions from seismic sources, Bull. Seism. Soc. Am., 50, 117–134, 1960.

390 Kubo, A., Fukuyama, E., Nonomura, K.: NIED seismic moment tensor catalogue for regional earthquakes around Japan: quality test and application, Tectonophysics, 356, 23-48, https://doi.org/10.1016/S0040-1951(02)00375-X, 2002.

Lee, W.H.K., Lahr, J.C.: Hypo 71 (revised): a computer program for determining hypocentre, magnitude and firs motion pattern of local earthquakes, USGS Open File Report 75-311, Menlo Park, 113 pp., 1975.

Lentas, K., Di Giacomo, D., Harris, J., Storchak, D.A.: The ISC Bulletin as a comprehensive source of earthquake source
395 mechanisms, Earth Syst. Sci. Data, 565-578, 2019.

Locati, M., Camassi, R., Rovida, A., Ercolani, E., Bernardini, F., Castelli, V., Caracciolo, C.H., Tertulliani, A., Rossi, A., Azzaro, R., D'Amico, S., Conte, S., Rocchetti, E.: Database Macrosismico Italiano (DBMI15). Istituto Nazionale di Geofisica e Vulcanologia (INGV), Roma, Italia, https://doi.org/10.6092/INGV.IT-DBMI15, 2016.

McKenzie, D.: Active tectonics of the Mediterranean Region, Geophys. J. R. Astr. Soc., 30, 109-185, doi.org/10.1111/j.1365-
400 246X.1972.tb02351.x, 1972.

Meletti C, Marzocchi W, D'Amico V, Lanzano G, Luzi L, Martinelli F, Pace B, Rovida A, Taroni M, Visini F, the MPS19 Working Group: The new Italian Seismic Hazard Model, Annals Geophys., 64, 1 -29, SE112 doi:10.4401/ag-8579 , 2021

Nakamura, W., Uchida, N., Matsuzawa, T.: Spatial distribution of the faulting types of small earthquakes around the 2011 Tohoku- oki earthquake: A comprehensive search using template events, J. Geophys. Res. Solid Earth, 121, 2591–2607,
405 https://doi.org/10.1002/2015JB012584, 2016.

Peruzza, L., Garbin, M., Snidarcig. A., Sugan, M., Urban. S., Renner, G., Romano, M.A.: Quarry blasts, underwater explosions and other dubious seismic events in NE Italy from 1977 till 2013, Boll. Geof. Teor. Appl., 56, 437-459, https://doi.org/10.4430/bgta0159, 2015.

Peruzza L., Iliceto V., Slejko D.: Some seismotectonic aspects of the Alpago-Cansiglio area (N.E. Italy), Boll.Geof. Teor. Appl., 31, 63-75, 1989.

Poli, M.E., Renner, G.: Normal focal mechanism in the Julian Alps and Prealps: seismotectonic implications for the Italian-Slovenian Border region, Boll. Geof. Teor. Appl., 45, 51-69, 2004.

Poli, M.E., Peruzza, L., Rebez, A., Renner, G., Slejko, D., Zanferrari, A.: New seismotectonic evidence from the analysis of the 1976-1977 and 1977-1999 seismicity in Friuli (NE Italy), Boll. Geof. Teor. Appl., 43, 53-78, 2002.

Pondrelli, S., Ekström, G., Morelli, A.: Seismotectonic re-evaluation of the 1976 Friuli, Italy, seismic sequence, J. Seism., 5, 73-83, 2001.

Pondrelli, S., Salimbeni, S.: Regional moment tensor review: an example from the European–Mediterranean Region, in Encyclopedia of Earthquake Engineering (pp. 1–15), Springer Berlin Heidelberg, https://doi.org/10.1007/978-3-642-36197-5_301-1, 2015.

Priolo, E., Barnaba, C., Bernardi, P., Bernardis, G., Bragato, P.L., Bressan, G., Candido, M., Cazzador, E., Di Bartolomeo, P., Durì, G., Gentili, S., Govoni, A., Klinc, P., Kravanja, S., Laurenzano, G., Lovisa, L., Marotta, P., Michelini, A., Ponton F., Restivo, A., Romanelli, A., Snidarcig, A., Urban, S., Vuan, A., Zuliani, D.: Seismic monitoring in northeastern Italy: A ten-year experience, Seismol. Res. Lett., 76, 446–454, https://doi.org/10.1785/gssrl.76.4.446, 2005.

Radulian M., E Popescu, A Bala, A Utale: Catalog of fault plane solutions for the earthquakes occurred on the Romanian territory, Romanian Journal of Physics, 47,663-686, 2002.

Reasenberg, P., Oppenheimer, D.: FPFIT, FPPLOT and FPPAGE: Fortran computer programs for calculating and displaying earthquake fault-plane solutions, Open-File Rep., 85-739, USGS, Menlo Park, 109 pp., 1985.

Restivo, A., Bressan, G., Sugan, M.: Stress and strain patterns in the Venetian Prealps (north-eastern Italy) based on focal-mechanism solutions, Boll. Geof. Teor. Appl., 57, 13-30, https://doi.org/10.4430/bgta0166, 2016.

Riggio, A., Russi, M.; 1984: Procedura di analisi ed elaborazione dei dati registrati da reti sismometriche locali. In: Finalità ed Esperienze della Rete Sismometrica del Friuli-Venezia Giulia, Reg. Aut. Friuli-Venezia Giulia, Trieste, Italy, pp. 53-74

Romano, M.A., Peruzza, L., Garbin, M., Priolo, E., Picotti, V.: Microseismic portrait of the Montello thrust (Southeastern Alps, Italy) from a dense, high-quality seismic network, Seismol. Res. Lett., 90, 1502–1517, 2019.

Rovida, A., Locati, M., Camassi, R., Lolli, B., Gasperini, P.: The Italian earthquake catalogue CPTI15. Bull. Earth. Eng., 18, 2953-2984, https://doi.org/10.1007/s10518-020-00818-y, 2020.

Rovida, A., Locati, M., Camassi, R., Lolli, B., Gasperini, P., Antonucci, A.: Catalogo Parametrico dei Terremoti Italiani (CPTI15), versione 3.0. Istituto Nazionale di Geofisica e Vulcanologia (INGV), https://doi.org/10.13127/CPTI/CPTI15.3, 2021.

RTS – Real Time Seismology : http://rts.crs.inogs.it/en/ , last accessed 23 November 2020.

440   Saikia, CK: Modified frequency-wavenumber algorithm for regional seismograms using Filon's Quadrature- Modeling of Lg waves in eastern North America, Geophys. J. Int., 118, 142-158, https://doi.org/10.1111/j.1365-246X.1994.tb04680.x, 1984.

Sandron, D., Rebez, A., Slejko, D.: Calibration of the duration magnitude for the north-eastern Italy Seismic Network (OX) on the basis of the revised local magnitudes of the Trieste Station, Boll. Geof. Teor. Appl., 59, 249- 266, https://doi.org/10.4430/bgta0237, 2018.

445   Saraò, A.: Seismic moment tensor determination at CRS: feasibility study, Open Report, OGS 2007/60-CRS/16, 43 pp., 2007.

Saraò, A.: Online catalogue of moment tensor solutions of earthquakes occurred in NE Italy and its surroundings in the period 2014– 2016, http://bit.ly/2jlxfvv, 2016, last access: 20 October 2020.

Saraò, A.: Seismic moment tensor solutions of Mw > 3.4 earthquakes occurred between 2002 and 2018 in the Southeastern Alps. Zenodo. http://doi.org/10.5281/zenodo.4298707, 2020.

450   Saraò, A., Sugan, M., Bressan, G., Renner, G., Restivo A.: Focal mechanisms of the Southeastern Alps and surroundings (Version 1.1) [Data set]. Zenodo. http://doi.org/10.5281/zenodo.4660412 ,2021.

Scognamiglio, L., Tinti, E., Quintiliani, M.: Time Domain Moment Tensor (TDMT) [Data set], Istituto Nazionale di Geofisica e Vulcanologia (INGV), https://doi.org/10.13127/TDMT, 2006.

Scognamiglio, E., Tinti, E., Michelini, A.: Real Time Determination of seismic moment tensor for the Italian Region, Bull.
455   Seism. Soc. Am., 99, 2223-2242, https://doi.org/10.1785/0120080104, 2009.

Serpelloni, E., Anzidei, M., Baldi, P., Casula, G., Galvani, A.: Crustal velocity and strain-rate fields in Italy and surrounding regions: new results from the analysis of permanent and non-permanent GPS networks, Geophys. J. Int. 161, 861–880, https://doi.org/10.1111/j.1365-246X.2005.02618.x, 2005.

Shearer, P. M.: Evidence from a cluster of small earthquakes for a fault at 18 km depth beneath Oak Ridge, southern California,
460   Bull. Seismol. Soc. Am., 88, 1327–1336, 1998.

Sirovich, L., Pettenati, F.: Source inversion of intensity patterns of earthquakes: a destructive shock in 1936 in northeast Italy, J. Geophys. Res., 109, B10309, https://doi.org/10.1029/2003JB002919, 2004.

Slejko, D., Carulli, G.B., Nicolich, R., Rebez, A., Zanferrari, A., Cavallin, A., Doglioni, C., Carraro, F., Castaldini, D., Iliceto, V., Semenza, E., Zanolla, C.: Seismotectonics of the Eastern Southern-Alps: a review, Boll. Geof. Teor. Appl., 31, 109-136,
465   1989.

Slejko, D., Peruzza, L., Rebez, A.: Seismic hazard maps of Italy, Annals. Geophys., 41, 183-214, https://doi.org/10.4401/ag-4327, 1998.

Slejko, D., Neri, G., Orozova, I., Renner, G., Wyss, M.: Stress field in Friuli (NE Italy) from fault plane solutions of activity following the 1976 main shock, Bull. Seism. Soc. Am., 89, 1037-1052, 1999.

470   Slejko, D.: What science remains of the 1976 Friuli earthquake?, Boll. Geofis. Teor. 530 Appl., 59, 327-350. doi:10.4430/bgta0224, 2018.

Sugan, M., Peruzza, L.: Distretti sismici del Veneto, Boll. Geof. Teor. Appl., 52, suppl., s3-s90, https://doi.org/10.4430/bgta0057, 2011.

Sugan, M., Renner, G., Bressan, G., Restivo, A., Saraò A.: First motion data and focal mechanism solutions of 108 earthquakes
475   occurred between 1928 and 2019 in the Southeastern Alps [Data set], Zenodo, http://doi.org/10.5281/zenodo.4284929, 2020

Udías, A., Buforn, E., Ruiz De Gauna, J.: Catalogue of focal mechanisms of European earthquakes, Department of Geophysics, Universidad Complutense, Madrid, pp. 274, 1989.

Viganò, A., Bressan, G., Ranalli, G., Martin, S.: Focal mechanism inversion in the Giudicarie–Lessini seismotectonic region (Southern Alps, Italy): Insights on tectonic stress and strain, Tectonophysics, 460, 106–115, https://
480   doi.org/10.1016/j.tecto.2008.07.008, 2008.

Viganò, A., Scafidi, D., Ranalli, G., Martin, S., Della Vedova, B., Spallarossa, D.: Earthquake relocations, crustal rheology, and active deformation in the central–eastern Alps (N Italy), Tectonophysics, 661, 81-98, https://doi.org/10.1016/j.tecto.2015.08.017, 2015.

Vannucci, G., Gasperini, P.: The new release of the database of Earthquake Mechanisms of the Mediterranean Area (EMMA
485   Version 2), Annals Geophys., 47(1), 307-334, with CD-ROM, https://doi.org/10.4401/ag-3277, 2004.

Wessel, P., Luis, J. F., Uieda, L., Scharroo, R., Wobbe, F., Smith, W. H. F., Tian, D.: The Generic Mapping Tools version 6, Geochemistry Geophysics Geosystems, 20, 5556–5564. https://doi.org/10.1029/2019GC008515, 2019.

Whitcomb, J. H.: Part I. A study of the velocity structure of the Earth by the use of core phases. Part II. The 1971 San Fernando earthquake series, focal mechanisms and tectonics, Ph.D. Thesis, California Institute of Technology, Pasadena, 1973.

490   Zoback, M.L.: First- and second-order patterns of stress in the lithosphere: the world stress map project, J. Geophys. Res., 97, 11703-11728, https://doi.org/10.1029/92JB00132, 1992.

Zuliani, D., Fabris, P., Rossi, G.; FReDNet: Evolution of a Permanent GNSS Receiver System, In: Cefalo R., Zieliński J., Barbarella M. (eds) New Advanced GNSS and 3D Spatial Techniques. Lecture Notes in Geoinformation and Cartography. Springer, Cham, https://doi.org/10.1007/978-3-319-56218-6_10, 123-137, 2018.

495

Figure 1: Map of the epicentres of the focal mechanisms reported in the catalogue (Saraò et al., 2021) presented in this paper. The epicentres of the focal mechanisms retrieved from the literature are indicated by the blue dots, and the newly computed FPS are indicated by the red dots. The 1976 Friuli earthquake (orange star) and the 1998 and 2004 Bovec earthquakes (yellow stars) are also shown. The map was generated by GMT software (Wessel et al., 2019).

500

Figure 2 - Overview of the focal mechanisms contained in our catalogue. The map was generated by GMT software (Wessel et al., 2019).

505
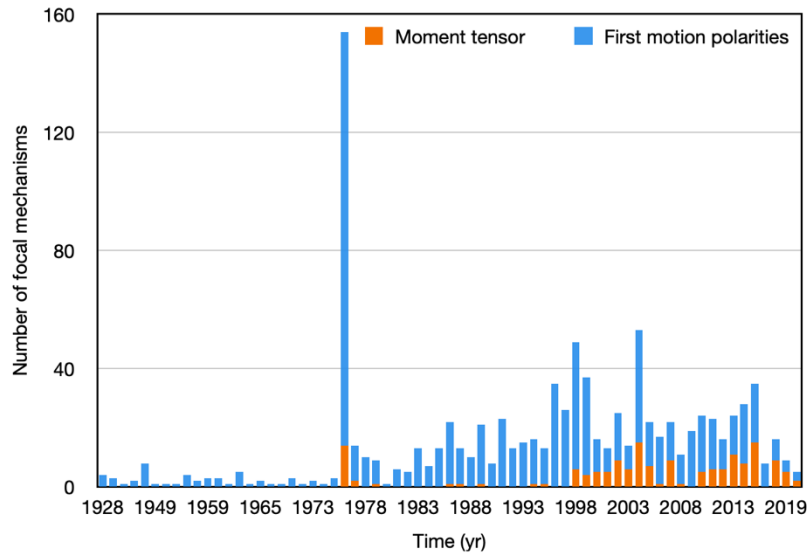
Figure 3 - Distribution in time of the fault plane solutions using a 1-year bin (year vs. number of fault plane solutions).
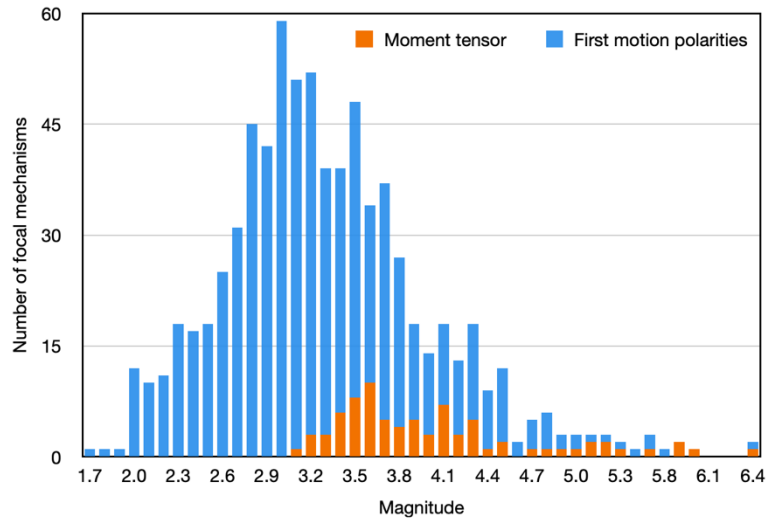
Figure 4 - Magnitude distribution of the fault plane solutions contained in the catalogue.

510
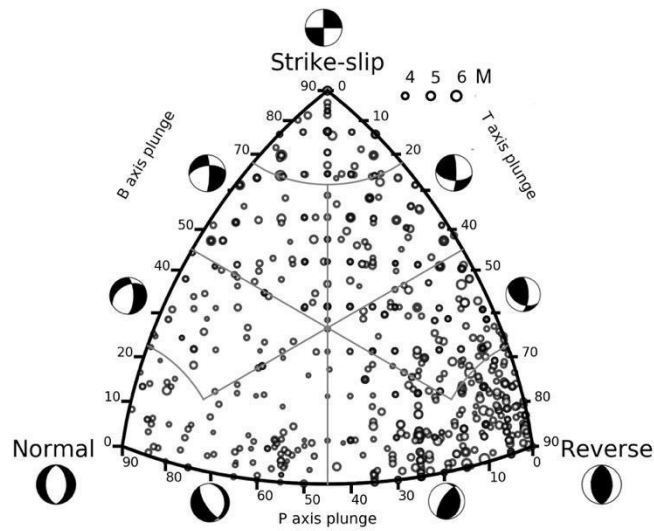
Figure 5 –   Focal mechanism classification of our catalogue plotted on the ternary diagram (Kaverina et al., 1996).
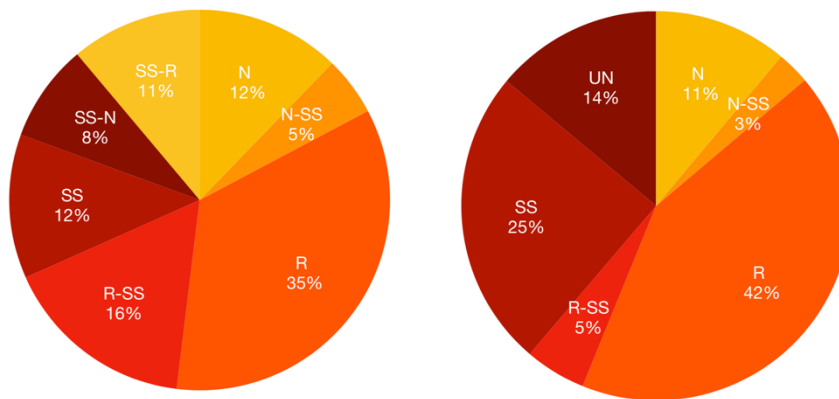
Figure 6 - a) Classification of the focal mechanism according to Álvarez-Gómez (2019) and b) Zoback (1992). N = Normal; N-SS = Normal - Strike-slip; SS-N= Strike-slip - Normal; SS = Strike-slip; SS-R= Strike-slip - Reverse; R-SS = Reverse - Strike-slip; R = Reverse; UN = Unknown.

515
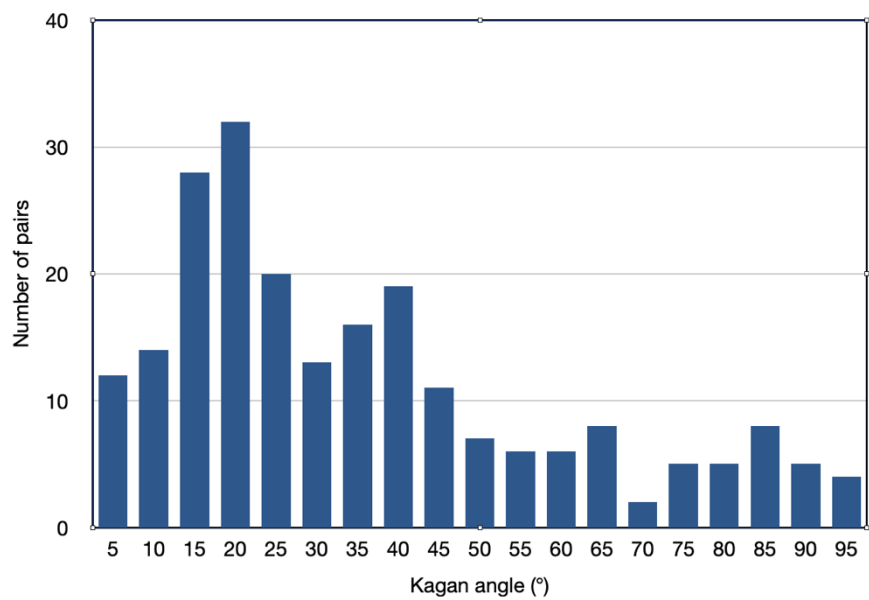
Figure 7 - Kagan angle between the preferred solution and the alternative FPS reported in our catalogue.

520

Table 1 - Parameters of the new FPS computed by first motion polarities (Sugan et al., 2020). Here we report: Date (yyyy-mm-dd), Time (hh:mm:ss), Lat. (latitude north in degrees) and Lon.(longitude east in degrees), Depth (km, * = fixed), M (magnitude), Str1, Dip1, Rak1 (strike, dip, rake of the first fault plane in degrees), Str2, Dip2, Rak2 (strike, dip, rake of the second fault plane in degrees), Ft (fault type according to Zoback 1992), FM (number of first motion polarities), STDR (station distribution ratio) and Misfit. Other details are given in the full catalogue (Saraò et al., 2021).

|	Date	Time	Lat.	Lon.	Depth	M	Str1	Dip1	Rak1	Str2	Dip2	Rak2	Ft	Fm	STDR	Misfit
1	1928-03-27	08:32:28	46.36	13.00	11.2	5.8	20	75	-10	113	80	-165	SS	23	0.7	0.1
2	1930-10-07	23:26:51	47.43	10.81	7*	5.3	0	60	150	106	64	34	TS	20	0.7	0.0
3	1931-12-25	11:41:11	46.30	13.04	13.5	5.2	65	65	40	315	54	149	TS	11	0.6	0.0
4	1936-10-18	03:10:05	46.09	12.47	13.3	5.6	100	55	120	235	45	54	TF	37	0.5	0.1
5	1936-10-19	07:05:55	46.15	12.46	8.8	4.6	80	50	110	230	44	68	TF	13	0.4	0.0
6	1949-02-03	22:29:01	46.51	13.14	10*	4.7	80	85	-150	347	60	-6	SS	16	0.8	0.1
7	1954-10-11	16:45:24	46.32	13.09	15.2	4.4	105	60	40	352	56	143	TS	11	0.7	0.0
8	1956-01-31	02:25:34	45.58	14.27	17.9	4.7	55	70	50	303	44	150	TS	13	0.6	0.0
9	1958-03-19	16:04:00	46.65	14.62	10.7	4.5	5	75	150	103	61	17	SS	13	0.6	0.0
10	1959-04-26	14:45:17	46.41	12.99	7.5	4.9	45	90	0	315	90	180	SS	33	0.5	0.1
11	1959-06-13	21:56:43	46.43	12.83	13.8	5	25	60	-150	279	64	-34	NS	16	0.4	0.1
12	1960-02-19	02:30:18	45.78	10.52	10.4	4.4	355	55	70	207	40	116	TF	20	0.5	0.1
13	1960-07-14	04:17:45	46.35	12.95	5.5	4.1	85	45	110	238	48	71	TF	13	0.4	0.0
14	1963-05-19	10:00:04	46.18	14.67	7.7	4.8	255	65	10	161	81	155	SS	33	0.5	0.1
15	1964-03-18	16:43:21	45.58	14.30	12.6	4.5	65	80	10	333	80	170	SS	23	0.7	0.1
16	1965-08-19	19:14:26	46.33	12.97	6.8	5	60	85	30	327	60	174	SS	16	0.8	0.0
17	1968-06-22	12:21:36	45.86	11.20	6.1	4.3	110	60	150	216	64	34	TS	30	0.7	0.1
18	1971-09-07	04:02:24	46.18	12.47	8.2	3.8	280	75	-150	182	61	-17	SS	14	0.6	0.0
19	1973-12-21	08:17:52	46.14	14.10	10.5	4	200	70	-30	301	62	-157	SS	22	0.4	0.2
20	1975-11-23	10:28:01	45.68	13.05	7*	3.6	200	75	-10	293	80	-165	SS	17	0.6	0.1
21	1976-02-27	09:58:48	45.81	13.08	8.5	3.4	155	10	-20	265	87	-99	U	21	0.5	0.0
22	1979-11-06	03:04:00	46.22	12.28	9.6	3.8	75	80	170	167	80	10	SS	25	0.7	0.1
23	1981-04-15	20:35:08	46.32	12.85	10.5	3.5	85	55	140	201	58	42	TS	28	0.6	0.2
24	1981-06-17	18:55:31	46.38	12.82	7.7	3.1	80	55	130	204	51	47	TF	17	0.6	0.0
25	1981-06-28	08:42:54	46.48	12.85	7.5	3.5	105	65	120	231	38	43	TF	29	0.6	0.1
26	1981-12-05	05:47:40	46.34	12.65	7.5	4.5	35	25	20	287	82	114	U	43	0.6	0.1
27	1982-05-18	15:10:45	46.40	12.45	9.3	3.2	95	55	-40	211	58	-138	NS	25	0.6	0.1
28	1982-09-29	22:35:26	46.22	12.48	9.0*	2.7	60	50	110	210	44	68	TF	26	0.5	0.1
29	1983-03-22	22:00:18	46.15	12.42	10.0	3	5	75	30	267	61	163	SS	27	0.6	0.2
30	1983-06-17	16:36:10	46.36	12.85	8.0	3.4	5	45	100	171	46	80	TF	35	0.6	0.2
31	1983-06-19	15:52:10	46.24	12.50	9.9	2.8	50	65	110	189	32	54	TF	25	0.5	0.1
32	1983-07-21	13:31:22	45.86	11.32	14.0	4.5	95	25	160	203	82	66	U	34	0.8	0.1
33	1984-07-08	07:58:49	45.63	12.19	17.2	3.6	5	65	-170	271	81	-25	SS	22	0.5	0.0
34	1984-10-25	13:58:55	45.61	14.24	12.2	3.5	0	10	90	180	80	90	TF	16	0.6	0.0

35	1984-10-29	13:29:26	46.26	12.51	10.9	3.3	105	35	80	297	56	97	TF	41	0.6	0.2
36	1984-12-15	10:55:10	46.28	12.60	10.0	3.7	70	60	110	214	36	59	TF	50	0.5	0.1
37	1985-02-08	01:45:52	46.50	12.78	6.1	3	115	80	150	211	61	12	SS	33	0.6	0.0
38	1985-02-08	21:10:40	46.49	12.78	7.0	2.7	25	80	20	291	70	169	SS	28	0.7	0.0
39	1985-05-05	17:55:31	46.34	12.62	11.3	2.9	235	75	140	337	52	19	SS	34	0.8	0.0
40	1985-06-18	04:52:56	45.82	11.00	12.5	3.6	95	60	140	208	56	37	TS	26	0.7	0.1
41	1985-07-09	23:09:48	46.51	12.72	7.0	2.4	20	70	50	268	44	150	TS	24	0.6	0.0
42	1985-08-04	06:59:12	46.48	12.57	8.0*	2.3	75	70	90	255	20	90	TF	21	0.4	0.0
43	1985-11-24	05:36:17	46.35	12.50	5.8	2.3	60	50	80	255	41	102	TF	21	0.5	0.2
44	1985-11-24	06:28:34	46.35	12.51	6.7	2.7	90	40	120	233	56	67	TF	33	0.5	0.1
45	1986-01-13	12:50:38	46.36	12.74	8.7	2.1	60	45	-130	290	57	-57	NF	27	0.5	0.1
46	1986-01-15	01:40:17	46.16	12.39	6.6	2.8	200	30	40	74	71	114	TF	33	0.5	0.2
47	1986-02-05	22:52:50	46.30	12.65	3.9	3.1	80	55	10	344	82	145	SS	35	0.7	0.0
48	1986-07-05	10:33:18	46.38	12.39	7.0	2.4	105	45	120	246	52	63	TF	26	0.5	0.1
49	1986-09-04	20:50:49	46.40	12.44	7.0	2.6	130	30	150	247	76	63	TF	28	0.5	0.2
50	1986-10-07	20:59:59	46.39	12.42	6.2	2.4	135	30	90	315	60	90	TF	34	0.6	0.1
51	1986-10-08	20:18:45	46.38	12.41	4.3	2.9	125	35	80	317	56	97	TF	38	0.6	0.0
52	1987-03-10	23:16:26	46.39	12.60	7.2	2.5	90	50	-120	312	48	-59	NF	23	0.5	0.1
53	1987-04-07	20:04:20	46.45	12.34	7.0*	3.6	60	40	20	314	77	128	U	52	0.6	0.2
54	1987-05-24	10:23:25	45.70	10.73	6.6	4.2	60	45	100	226	46	80	TF	46	0.5	0.2
55	1987-06-25	07:49:27	46.28	12.59	8.1	2.6	60	90	-80	150	10	-180	U	24	0.4	0.1
56	1987-07-10	08:09:28	45.98	10.92	8.7	3.7	85	55	140	201	58	42	TS	39	0.7	0.2
57	1987-10-20	00:33:26	46.30	12.63	3.7	3.4	275	90	-20	5	70	-180	SS	47	0.7	0.1
58	1987-10-31	13:09:41	46.35	12.83	8.6	2.8	20	45	120	161	52	63	TF	40	0.6	0.0
59	1987-12-04	14:45:12	45.89	10.60	7.1	3.8	125	80	120	232	31	19	U	35	0.6	0.1
60	1987-12-15	11:29:25	46.17	12.37	10.5	2.9	0	15	60	211	77	98	TF	32	0.6	0.1
61	1988-04-05	21:28:00	46.28	12.54	7.6	2.6	15	70	-170	282	81	-20	SS	29	0.6	0.1
62	1988-12-06	18:13:22	46.33	12.63	6.6	2.8	35	55	60	260	45	126	TF	27	0.5	0.2
63	1989-03-18	12:04:51	45.85	12.81	9.7	3.2	160	55	-40	276	58	-138	NS	28	0.6	0.0
64	1989-04-29	06:27:00	46.18	12.80	7.0*	2.8	90	60	-60	221	41	-131	NF	18	0.5	0.1
65	1989-05-27	15:56:03	46.39	12.90	12.0	3.2	40	60	40	287	56	143	TS	13	0.5	0.2
66	1989-08-14	04:11:56	46.04	13.67	10.7	2.3	180	70	-70	313	28	-133	NF	18	0.5	0.0
67	1989-08-14	04:26:25	46.02	13.66	12.9	2.9	180	70	-70	313	28	-133	NF	22	0.6	0.1
68	1989-08-14	10:51:17	46.02	13.66	13.4	3	175	65	-50	292	46	-144	NF	22	0.6	0.1
69	1989-08-14	12:43:04	46.02	16.65	12.6	2.9	225	85	-70	328	21	-166	U	22	0.7	0.0
70	1990-02-04	08:13:13	46.21	13.66	13.2	2.4	180	45	-50	310	57	-123	NF	17	0.6	0.0
71	1990-02-04	09:22:15	46.20	13.66	13.3	2.6	185	45	-40	306	63	-127	NF	15	0.6	0.0
72	1990-06-28	18:56:59	45.94	12.36	11.3	2.5	240	85	160	332	70	5	SS	15	0.7	0.0
73	1990-06-28	19:30:10	45.93	12.38	11.2	3.2	60	90	-170	330	80	0	SS	21	0.6	0.0
74	1992-02-24	21:31:43	46.30	12.46	9.7	2.6	60	70	120	181	36	36	TF	26	0.5	0.3
75	1992-03-11	15:40:32	45.95	14.33	10.3	3.9	30	80	0	300	90	170	SS	33	0.6	0.1
76	1992-07-13	09:40:58	46.06	13.68	12.3	2.3	280	85	-130	184	40	-8	U	16	0.5	0.1
77	1993-01-12	11:07:00	46.40	12.46	11.6	2.2	305	75	-170	212	80	-15	SS	16	0.7	0.1

78	1993-02-27	16:26:00	46.26	12.51	9*	2.1	120	55	50	356	51	133	TF	13	0.7	0.0
79	1993-08-23	23:12:50	46.29	12.55	5.8	1.9	120	60	-30	226	64	-146	NS	16	0.7	0.2
80	1993-09-12	21:50:16	46.28	12.63	7.6	2	60	65	40	310	54	149	TS	19	0.6	0.2
81	1993-12-01	10:10:14	46.36	12.75	11.0	2.7	5	55	40	249	58	138	TS	16	0.7	0.1
82	1994-05-25	23:32:31	46.01	13.51	7.1	2.9	145	85	-130	49	40	-8	U	25	0.5	0.2
83	1994-12-05	21:14:09	46.41	12.68	10.8	2.6	35	80	20	301	70	169	SS	24	0.6	0.2
84	1996-02-10	04:02:55	45.82	11.15	14.8	3.1	65	50	80	260	41	102	TF	38	0.5	0.1
85	1997-03-17	22:45:12	46.44	13.03	7.6	3.1	90	20	60	302	73	100	TF	27	0.6	0.2
86	1997-06-16	14:38:26	45.88	11.99	12.6	2.8	55	25	-60	203	69	-103	NF	28	0.6	0.2
87	1997-06-19	16:54:09	45.94	12.25	9.6	2.5	115	75	130	222	42	23	TS	16	0.5	0.2
88	1997-07-06	22:28:58	45.57	10.50	11.6	3.5	220	70	-50	332	44	-150	NS	23	0.4	0.1
89	1997-07-25	15:54:18	45.87	11.12	13.7	3.3	135	50	130	262	54	53	TF	30	0.6	0.1
90	1997-10-18	19:58:45	45.10	12.19	24.5	3.2	130	70	20	33	71	159	SS	34	0.7	0.2
91	1998-12-26	19:30:58	45.86	11.42	15.3	3.6	90	60	100	251	31	73	TF	46	0.6	0.1
92	1999-01-05	03:22:15	45.76	10.79	5.0	3.3	35	85	40	301	50	173	U	39	0.4	0.1
93	1999-06-30	19:11:58	45.27	11.96	12.6	3.6	25	55	80	222	36	104	TF	33	0.5	0.1
94	2000-09-08	05:49:26	45.72	10.83	8.8	3.2	5	25	90	185	65	90	TF	25	0.5	0.2
95	2001-12-10	07:58:40	45.88	11.77	13.8	3.3	200	50	-20	303	75	-138	NS	29	0.6	0.2
96	2001-12-18	17:43:56	45.98	11.10	12.7	3.2	210	70	-10	303	81	-160	SS	36	0.6	0.2
97	2018-01-17	10:22:20	46.31	13.57	10.6	3.8	105	80	170	197	80	10	SS	35	0.7	0.1
98	2018-01-19	17:39:43	46.42	13.03	13.8	3.5	355	65	70	216	32	126	TF	36	0.6	0.1
99	2018-02-25	08:16:30	46.37	12.59	9.9	3.7	30	45	50	260	57	123	TF	35	0.6	0.1
100	2018-02-25	14:36:26	46.36	12.59	9.1	3.1	90	75	-160	355	71	-16	SS	32	0.7	0.1
101	2018-05-09	21:48:03	46.29	13.11	7.2	3.7	65	35	80	257	56	97	TF	38	0.5	0.1
102	2018-08-11	03:30:39	46.34	13.04	11.1	3.9	60	60	80	259	31	107	TF	40	0.5	0.1
103	2018-08-11	03:54:58	46.33	13.03	13.6	3.6	60	60	80	259	31	107	TF	38	0.5	0.1
104	2018-11-10	07:59:36	46.29	13.21	11.1	3	95	40	80	288	51	98	TF	33	0.5	0.1
105	2018-11-19	14:23:46	46.16	13.44	16.3	2.7	60	70	40	314	53	155	TS	34	0.6	0.1
106	2019-05-09	03:14:23	45.951	13.766	17.4	3.3	120	85	-180	30	90	-5	SS	36	0.6	0.2
107	2019-06-14	13:57:24	46.396	12.99	8.4	4	60	40	80	253	51	98	TF	32	0.5	0.1
108	2019-09-22	12:58:43	46.443	12.998	13.8	3.8	15	30	30	258	76	117	TF	31	0.6	0.1

530

Table 2 - Parameters of the new focal mechanism solutions computed by the moment tensor (Saraò, 2020). Date (yyyy-mm-dd), Time (hh:mm:ss), Lat. (latitude north) and Lon. (longitude east in degrees), Depth (km), Ml (local magnitude), MD (duration magnitude), Mw (moment magnitude), Str1, Dip1, Rak1 (strike, dip, rake of the first fault plane in degrees), Str2, Dip2, Rak2 (strike, dip, rake of the second fault plane in degrees), Ft (fault type according to Zoback 1992) and Q (quality inversion parameter; 4=best solution). Other details are given in the full catalogue (Saraò et al., 2021).

	Date	Time	Lat.	Lon.	Depth	Ml	M$_D$	Mw	Mo (dyn cm)	Str1	Dip1	Rak1	Str2	Dip2	Rak2	Ft	Q
1	2002-11-13	10:48:04	45.56	10.15	10		4.2	4.1	1.36E+22	63	80	118	172	30	21	U	2
2	2004-07-12	13:04:00	46.30	13.63	4		5.1	5.1	4.57E+23	220	83	-9	311	81	-173	SS	4
3	2005-01-14	07:58:13	46.19	14.02	12		4.1	3.8	6.08E+21	201	68	-29	303	63	-156	SS	4
4	2005-01-14	08:05:19	46.20	14.04	14		3.9	3.6	3.00E+21	216	90	1	126	89	180	SS	3
5	2005-04-24	18:34:01	45.56	14.29	8		4.5	4.0	1.05E+22	155	77	-165	62	75	-13	SS	4
6	2007-01-01	14:59:45	46.51	14.23	10		3.9	3.8	5.10E+21	85	50	91	263	40	89	TF	3
7	2007-02-05	08:30:04	45.11	15.00	10		4.4	4.3	2.92E+22	224	72	-26	322	66	-161	SS	3
8	2007-05-02	12:49:13	46.50	14.47	8		3.7	3.6	3.12E+21	80	55	81	275	36	102	TF	2
9	2007-05-19	16:19:40	47.17	10.61	14		3.7	3.7	3.68E+21	338	89	-5	68	85	-179	SS	4
10	2007-08-13	13:58:30	45.18	13.45	12	3.6		3.6	3.16E+21	168	84	140	263	51	8	U	2
11	2008-10-21	08:12:39	45.72	14.18	8	3.6		3.4	1.50E+21	89	61	85	280	29	100	TF	1
12	2010-01-15	14:20:54	45.78	14.22	16	4.0		3.5	1.91E+21	166	79	-146	68	57	-13	SS	3
13	2010-09-15	02:21:18	45.62	14.27	8	3.9		3.6	3.33E+21	161	74	161	256	72	17	SS	4
14	2010-09-15	02:23:14	45.62	14.27	8	3.9		3.5	1.96E+21	256	77	24	160	67	166	SS	4
15	2010-10-19	00:38:29	47.36	11.64	10	4.0		3.5	1.91E+21	264	65	98	66	27	73	TF	2
16	2011-09-13	18:35:24	45.90	12.05	10	3.7		3.4	1.50E+21	84	69	99	241	23	68	TF	3
17	2011-10-29	04:13:34	45.71	10.96	10	4.4		4.0	9.74E+21	245	51	79	81	40	103	TF	3
18	2012-01-24	23:54:46	45.55	11.00	10	4.2		4.0	1.18E+22	199	86	29	107	61	176	SS	3
19	2012-05-29	18:28:04	45.06	11.05	6	3.8		4.0	1.17E+22	265	68	83	102	23	106	TF	4
20	2012-06-09	02:04:56	46.20	12.47	6	4.3		4.1	1.86E+22	54	69	92	227	21	84	TF	4
21	2012-12-03	04:36:00	46.23	14.81	18	4.2		3.9	8.22E+21	47	78	24	311	66	167	SS	3
22	2013-02-02	13:35:33	46.48	14.63	4	4.3		4.2	2.06E+22	96	60	58	328	43	133	TF	3
23	2013-02-12	18:12:25	46.28	12.58	18	3.8		3.7	3.66E+21	234	51	64	91	45	118	TF	3
24	2013-06-16	20:04:58	45.77	14.84	2	4.0		3.7	4.30E+21	253	53	59	117	47	124	TF	4
25	2013-07-30	12:58:28	45.00	15.10	16	4.7		4.3	2.71E+22	212	86	17	121	73	176	SS	4
26	2013-08-24	13:59:01	46.21	12.55	10	3.6		3.5	2.04E+21	55	71	93	225	20	81	TF	3
27	2014-04-22	08:58:27	45.65	14.24	12	4.7		4.4	4.43E+22	249	87	-7	340	83	-177	SS	4
28	2014-05-29	07:24:18	46.10	13.86	12	3.8		3.6	2.79E+21	225	72	-22	322	69	-160	SS	3
29	2015-01-30	00:45:49	46.39	13.15	12	4.1		3.9	8.95E+21	53	81	72	297	20	153	U	4
30	2015-05-12	02:02:50	45.89	12.05	8	3.5		3.5	2.16E+21	59	69	85	254	21	104	TF	3
31	2015-05-15	05:35:47	45.88	12.06	6	3.6		3.5	2.23E+21	76	74	96	235	17	70	TF	3
32	2015-08-01	20:47:52	45.90	10.78	2	3.8		3.5	2.08E+21	355	77	32	257	59	165	SS	3
33	2015-08-18	20:10:02	45.89	11.90	12	3.6		3.4	1.57E+21	70	83	82	298	11	137	U	3
34	2015-08-29	18:47:04	46.31	13.60	6	4.3		4.1	1.56E+22	82	65	66	310	34	132	TF	3
35	2015-11-01	07:52:32	45.83	15.64	6	4.8		4.3	3.10E+22	273	61	83	106	30	102	TF	4

36	2015-11-21	11:52:38	46.43	12.71	6	3.5		3.6	2.49E+21	243	51	100	47	40	78	TF	2
37	2017-06-04	18:00:57	45.65	10.71	6	3.7		3.4	1.31E+21	245	51	112	33	44	66	TF	2
38	2017-07-21	17:03:56	45.65	10.70	6	3.4		3.4	1.44E+21	220	77	66	102	27	150	TF	1
39	2017-09-06	12:22:30	46.27	11.99	6	3.6		3.6	2.45E+21	300	78	148	38	59	14	SS	3
40	2018-01-17	10:22:20	46.32	13.58	8	3.8		3.8	5.31E+21	32	77	15	299	75	167	SS	3
41	2018-02-25	08:16:29	46.37	12.60	10	3.7		3.7	3.56E+21	8	88	-16	98	74	-178	SS	3
42	2018-08-11	03:30:39	46.34	13.07	8	3.9		3.7	3.88E+21	52	75	55	301	38	154	U	3
43	2018-12-05	16:23:59	45.69	14.28	8	3.8		3.5	2.11E+21	30	75	-62	146	31	-150	NS	1